ADVANCED ELECTRONIC MATERIALS
www.advelectronicmat.de

Contact Resistivity in Edge-Contacted Graphene Field Effect Transistors

*Sungwon Lee, Hyungyu Choi, Inyong Moon, Hoseong Shin, Kenji Watanabe, Takashi Taniguchi, and Won Jong Yoo**

A great challenge is presented when metals have contact with a 2D semiconducting material because the contact resistances (R_c) induced at the metal-graphene interfaces hinder the performances of 2D devices, and therefore low resistance Ohmic contacts need to be developed to achieve unique and high performance of the 2D devices. This study demonstrates that edge-contacted graphene devices of multiple stacked 2D hetero-structures with hexagonal boron nitride (hBN) exhibit superior performances in carrier transport across channel and contact regions, compared to surface-contacted devices. In surface-contacted graphene devices, R_c and contact resistivity (ρ_c) are calculated by applying the modified transfer length (L_T^*) obtained from the contact-end-resistance method, while R_c and ρ_c in edge-contacted graphene devices are estimated by replacing the L_T^* with the thickness of graphene. The edge-contacted device is fabricated via a controlled plasma etching that allows each layer of graphene and hBN consisting hetero-structures to be removed evenly at a uniform speed. Four-point probe measurements are conducted in addition to transmission line method and confirms that ρ_c is lower for edge contact than surface contact. ρ_c of a graphene edge-contacted device (≈10 Ω μm^2) is much lower than that of a surface-contacted device (≈230 Ω μm^2).

1. Introduction

Contact resistance (R_c) at the metal-graphene interface is a critical device parameter that can make it difficult to reveal the unique quantum mechanical properties of graphene devices,[1–5] being dependent on various processing parameters; e.g., the work function of contact metals (Φ_M),[6–11] the method to form metal contacts (surface,[12] edge,[13–15] and sandwich contacts[6,16,17]), the number of graphene layers,[18] the density of defects at the surface, the electrical bias applied to the graphene devices. According to other references, low R_c on edge-contacted graphene devices was reported: e.g., by n-type doping[19] or forming carbide with titanium (Ti) and palladium (Pd).[20] Also, very low R_c was obtained by incorporating chemical elements such as O and S into the contact region, where oxygen (O) and sulfur (S) were used to replace hydrogen (H) and fluorine (F).[21] Other reported methods include the formation of cuts and holes in graphene flakes.[22,23] There also have been reports on the decrease of R_c when metals are in contact with edges or defects of graphene, attributed to covalent bonding and short bonding distance.[13,14,18,24–28]

In general, R_c for semiconductor devices is determined by transmission line measurement (TLM) and four-point probe measurement (4PPM). TLM is a very efficient method to measure R_c between metal and semiconductor material interfaces. In TLM, several channels are configured in the device with linearly increased spacing (referred to channel length (L_{ch}) hereafter). Total resistances (R_T) extracted from each channel are then plotted as a function of L_{ch}, with the y-intercept value corresponding to R_c as shown in the following Equation (1).

$$R_T = 2R_C + \left(\frac{R_{sh}}{W}\right)L_{ch} \quad (1)$$

More importantly, TLM gives rise to a significant error when calculating transfer length (L_T) in the surface-contacted graphene field effect transistors (FETs). According to the conventional TLM, contact resistivity (ρ_c) of the graphene channel is assumed to be the same as that of graphene under metal. However, these two regions are distinctly different and therefore they need to be considered differently. In the modified TLM, the so-called contact-end-resistance (CER) method is realized by the strict separation of these two aforementioned parts.[9,10] Modified transfer lengths (L_T^*) were obtained from the modified TLM (referred to CER method hereafter) which takes into account the change in channel resistance (R_{ch}) underneath a contact metal, and thus obtained L_T^* were used to calculate the effective contact area.

Here, a plasma processing is adopted for TLM, related to edge-contacted graphene FETs. It is well known that plasma treatments have been widely used to achieve nanoscale patterns due to its anisotropic etching capability between vertical and

S. Lee, H. Choi, I. Moon, H. Shin, W. J. Yoo
Department of Nano Science and Technology
SKKU Advanced Institute of Nano-Technology (SAINT)
Sungkyunkwan University
2066 Seobu-ro, Jangan-gu, Suwon, Gyeonggi-do 16419, Republic of Korea
E-mail: yoowj@skku.edu
K. Watanabe, T. Taniguchi
National Institute for Materials Science
1-1 Namiki, Tsukuba 305-0044, Japan

The ORCID identification number(s) for the author(s) of this article can be found under https://doi.org/10.1002/aelm.202101169.

DOI: 10.1002/aelm.202101169

lateral directions and its environment-friendliness, compared to wet etching. Nevertheless, the plasma treatments have limitations in securing a processing margin of 2D devices due to the ultra-thinness of 2D materials. Besides, plasma etching of few-layer graphene-based hetero-structure presents difficulty in successively treating them because carbon-based graphene is very sensitive to plasma radicals containing oxygen and fluorine, while other interfacing 2D layers such as hexagonal boron nitride (hBN) show very different plasma reactions and etching rates from graphene. Therefore, it is required to study plasma etching properties of the hetero-structured graphene devices so as to realize high performance functional 2D devices. Unlike simply depositing a metal on the surface of the channel materials, the edge contact is realized by contacting the metal to the edge of graphene, usually by performing O_2 plasma treatment that etches graphene. A part of the few-layer graphene was used to prepare surface-contacted devices while another part was covered by hBN to prepare edge-contacted devices for the purpose of preventing surface contact. Edge-contact devices were fabricated by plasma etching, after analyzing etching properties of each of hBN and graphene using different plasma gases. By analyzing time dependent etching results of each material, we optimized the ratio of plasma gases consisting of carbon tetrafluoride (CF_4)[29,30] and O_2[31–34] so as to obtain a desired etching profile of a hetero-structure consisting of hBN and graphene. The graphene/hBN stack thus etched by using mixed plasma gases showed a linear sidewall profile which could be used for forming edge-contacted hetero-structure devices.

Alternatively, R_c can be determined in 4PPM devices by measuring voltage drop between two inner probes while flowing constant current between two outer probes. In this case, the two inner voltage probes are patterned shorter than the outer probes so that they have negligibly little effects on the current flow in the channel material. To obtain accurate 4PPM results, channel region also needs to be redefined with a rectangular shape so as to minimize the influence of voltage probes on the current flow in the channel region (see **Figure 1**). Although this channel definition process adds complexity to the device fabrication, the thus designed 4PPM can eliminate origins causing the erroneous results of R_c.[35]

In this study, we investigate R_c and ρ_c of graphene devices obtained by using large graphene flakes exfoliated on the same substrate that can produce both surface- and edge-contacted FETs. For accurate analysis of each contact, we introduce the CER method to obtain L_T^* of the surface-contacted device, yielding a corresponding ρ_c. For determining the effective contact area, we treat L_T^* of the surface-contacted device equivalently to the graphene thickness of the edge-contacted device. To ensure to obtain reliable ρ_c of each device, the analyses based on 4PPM are conducted as well as TLM.

2. Results and Discussion

2.1. Device Structural Characteristics of the Surface- and Edge-Contacted Graphene Devices

We fabricated surface- and edge-contacted graphene devices with TLM and 4PPM designs and analyzed the device structural characteristics of the devices as shown in Figure 1a,b. The area shown in purple channel represents a few-layer graphene which is used to form a surface-contacted device without hBN, whereas the area shown in blue flake in Figure 1a represents hBN covering a few-layer graphene which is used to form an edge-contacted device. Figure 1b is a schematic of the device structures formed by the surface and edge contacts. Here, Pd is used to form edge contact with graphene, because high current flows through the graphene devices with Pd which shows strong chemisorption based bonding when it is in contact with graphene.[12,18,36] Our graphene sample consists of few-layer, and its thickness was determined by atomic force microscopy (AFM) and Raman spectroscopy as shown in Figure 1c,d. As plotted in Figure S1 (Figure S1, Supporting Information), etching rates of graphene and hBN showed different trends from each other as a function of CF_4 gas concentration. Graphene was easily etched by oxygen radicals generated in capacitively coupled plasma (CCP) while hBN was readily etched by fluorine radicals originated from CF_4 gas. When CF_4 concentration increased from 2% to 10%, the etching rate of hBN was sharply increased while that of graphene was gradually decreased. We found that hBN and graphene could have the same etching rate when the fluorine concentration was ≈3%. This plasma etching condition was used extensively for our device processing of various multilevel hetero-structures consisting of hBN and graphene. Inset of Figure S1 (Supporting Information) shows a schematic image of plasma etching process conducted on a hetero-structure consisting of few-layer hBN and graphene. As the result, hetero-structure stacks were etched with a constant speed, by using mixture plasma gases composed of CF_4 and O_2; the top of the hBN layer was etched by the optimized mixture gases, and the bottom graphene layer was then continuously etched by the same gases. The analytical method to determine etching rate of each 2D material in the device stack structures is described as shown in Figure S2 (Supporting Information), which can be used for developing etching process of 2D materials in the case where it is difficult to measure difference in step heights before and after etching due to their ultra-thinness, in contrast to the step heights commonly measured for conventional electronic materials such as silicon (Si), silicon dioxide (SiO_2), aluminum (Al), photoresist. In addition, Raman spectra when this plasma treatment was treated on hBN and graphene using the mixed gas are shown in Figures S3 and S4 (Supporting Information). The etching profile observed by transmission electron microscopy (TEM) as well as electron energy loss spectroscopy (EELS) is shown in Figure 1f. The upper image in Figure 1f shows the etching profile of the edge-contacted graphene device consisting of graphene, hBN, and Pd. The image below in Figure 1f shows qualitative analysis performed by EELS. All regions of the device are distinguished by red, green, and blue colors.

2.2. R_c and ρ_c Obtained From Conventional and Modified TLM

Here, we employ the CER method.[9,10] Note that graphene sheet resistance under the contact metal (R_{sk}) and that of the channel (R_{sh}) are different. Using the CER method illustrated in **Figure 2**a, we were able to obtain contact-front-resistance

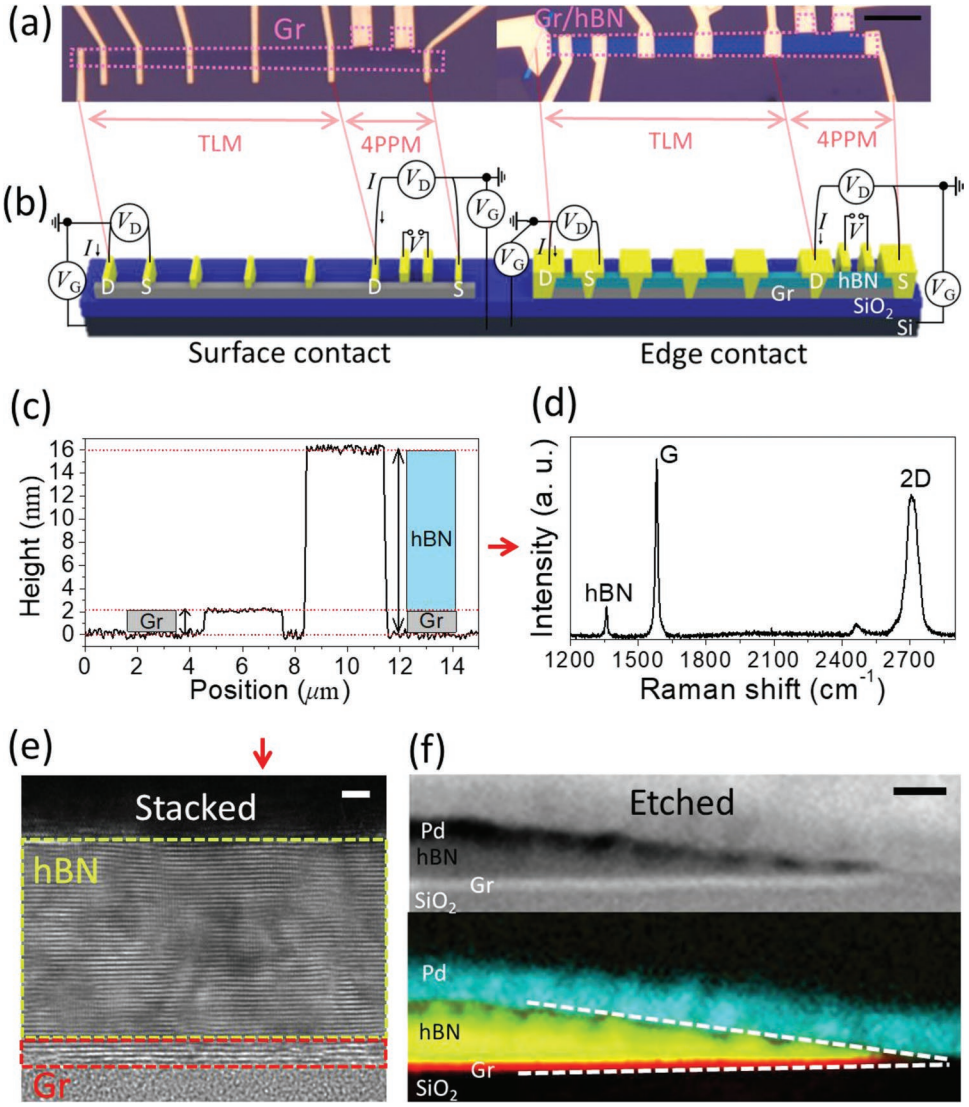

Figure 1. Fabrication of the surface- and edge-contacted graphene devices. a) Optical microscope image of surface- (graphene only) and edge-contacted (graphene covered by hBN) devices including TLM and 4PPM structures. (Scale bar = 10 μm) b) Schematic image of the devices. c) Thicknesses of the graphene and 2D hBN measured by AFM. d) Raman spectrum of the heterostructure. e) Cross-sectional TEM image of the heterostructure. (Scale bar = 2 nm) f) Cross-sectional TEM and EELS images of edge-contacted graphene device (Scale bar = 10 nm.).

(R_{CF}), contact-end-resistance (R_{CE}), and L_T^*. Figure 2a shows the CER method performed by using a TLM device structure. I_{12} is current measured between 1 and 2, and V_{23} is voltage applied between 2 and 3. In this way, we can calculate both contact front and end resistances from our graphene FETs: $R_{CF} = V_{12}/I_{12}$ and $R_{CE} = V_{23}/I_{12}$. Figure 2b shows a schematic with a related circuit diagram used to calculate a L_T^* from the TLM data shown in Figure S5 (Supporting Information). As mentioned above, R_{ch} is different from that of the graphene covered by the metal, requiring modification of the conventional TLM method so as to extract an accurate L_T^*. R_{CF} and R_{CE} are calculated as follows.[9,10,37] The obtained R_{CF} and R_{CE} are shown in Figure 2c.

$$R_{CF} = \frac{V(x=0)}{I(x=0)} = \frac{\sqrt{R_{sk}\rho_c}}{W}\coth\left(\frac{L}{L_T^*}\right) = \frac{\rho_c}{WL_T}\coth\left(\frac{L}{L_T^*}\right) \quad (2)$$

$$R_{CE} = \frac{V(x=L)}{I(x=0)} = \frac{\sqrt{R_{sk}\rho_c}}{W}\sinh\left(\frac{L}{L_T^*}\right) = \frac{\rho_c}{WL_T}\sinh\left(\frac{L}{L_T^*}\right) \quad (3)$$

Using these Equations (2) and (3), we obtained L_T^*, ρ_c, and R_{sk}. In conventional TLM, L_T is obtained from Equation (1), by assuming $R_{sk} = R_{sh}$. However, L_T* as a modified transfer length should be obtained from $R_{total} = \frac{R_{sh}}{W}\left(L + 2\left(\frac{R_{sk}}{R_{sh}}\right)L_T^*\right)$ when $R_{sk} \neq R_{sh}$, where $L_T^* = \sqrt{\rho_c/R_{sk}}$ and is plotted as shown in Figure 2d.

Figure 3 shows the electrical results obtained from an edge-contacted graphene device. Figure 3a shows transfer curves obtained from the device with TLM design, in which L_{ch} was increased with a ≈2 μm interval, being ≈2.6, 4.6, 6.6, 8.7, 10.6, and 15.7 μm. In Figure 3a, it is noted that the transfer curves of few-layer graphene devices do not show a very sharp V-shape. Here, the sharpness of the curve can be quantized by

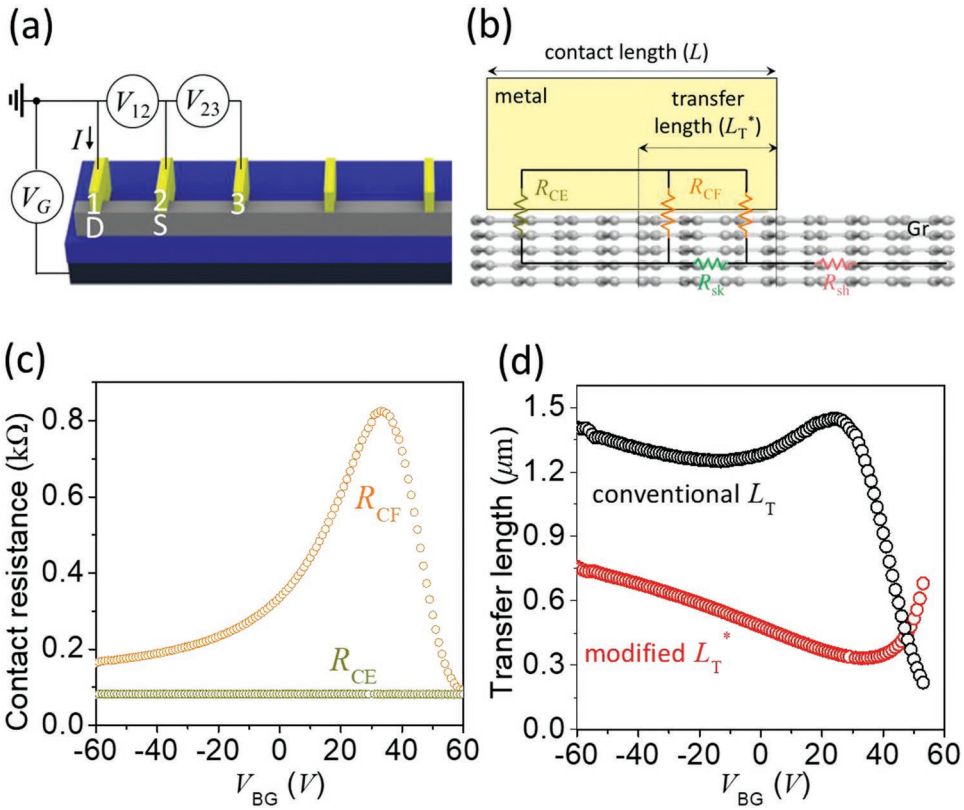

Figure 2. A setup to obtain a L_T^* from the CER method on a surface-contacted graphene device. a) A schematic image of the CER and TLM device. b) A schematic of surface-contacted CER device showing the differences between R_{CF} and R_{CE} at the interface of graphene and metal and between R_{sk} and R_{sh} in graphene channel. c) The difference of R_c obtained from R_{CF} and R_{CE}. d) L_T^* obtained from R_{CF} and R_{CE} are compared to L_T.

conductance ($\partial I_D/\partial V_D$) or transconductance ($\partial I_D/\partial V_G$). This could be due to two reasons. First, since continuous etching by a mixed gas was performed on the hBN/graphene heterostructure in this study, the electrical performance of graphene could be affected accordingly. Since fluorine containing etching gases could react with graphene for tens of minutes, some fluorine can be incorporated into graphene with a high conductivity, resulting in the decrease of the conductivity after etching.[38] The thicker the graphene, the more immune to fluorine; however, the degradation of the electrical performance is inevitable. When the period of plasma treatment was reduced to < 1 min to suppress the degradation of electrical conductance, low R_c values were yielded. The second reason is that the transfer curve of a monolayer graphene shows the highest on-off ratio, transconductance, and lowest off-conductance.[39] It is worth while noting that, the on-off ratio decreases and the slope of the transfer curve becomes gentle as the thickness increases.

Graphs plotted with TLM to measure R_c are shown in Figure 3b and Figure S5b (Supporting Information). It was obvious that R_T increases with L_{ch}; however, some deviations from a linear behavior were observed in the TLM results, presumably due to changes in patterns drawn by electron beam lithography (EBL) and chemical reaction between graphene and a contact metal deposited by electron beam deposition (EBD).[35,40] When the TLM devices were prepared, polymeric materials such as polymethyl methacrylate (PMMA) used as a mask for EBL pattering and sloped sidewall profiles formed by plasma etching could be responsible for the changes in pattern size. In Figure 3b and Figure S5b (Supporting Information), y-intercept values representing R_c were extracted from linear fitting of data obtained from each back-gate voltage. Yielded R_c show minimum values of 646 and 308 Ω μm as shown in Figure 3c and Figure S5c (Supporting Information) respectively. However, Figure 3c shows R_c as a function of back gate bias respectively, with a higher minimum R_c than surface-contacted devices. It could be seen that the changes in R_c were dependent on the back gate voltage and the effective cross-sectional area of current flow. It is shown that the mobility of graphene tends to decrease linearly as the temperature increases. This suggests that the higher the temperature, the more it is limited by phonon scattering as shown in Figure 3e,f.[36]

2.3. Comparison of R_c and ρ_c Measured by TLM and 4PPM

R_c of graphene FETs was calculated using TLM. However, in 4PPM, two probes are used to flow constant current, while the other two probes are used to measure the voltage drop induced from R_{ch}. Therefore, R_c can be estimated accurately. On the other hand, in two-point probe measurement (2PPM), R_{ch} and R_c cannot be separated, and therefore ρ_c cannot be estimated. We re-investigated R_c by performing 4PPM to confirm the results estimated by TLM. Additionally, we accurately measured L_{ch} and channel width (L_W), and applied the measured values

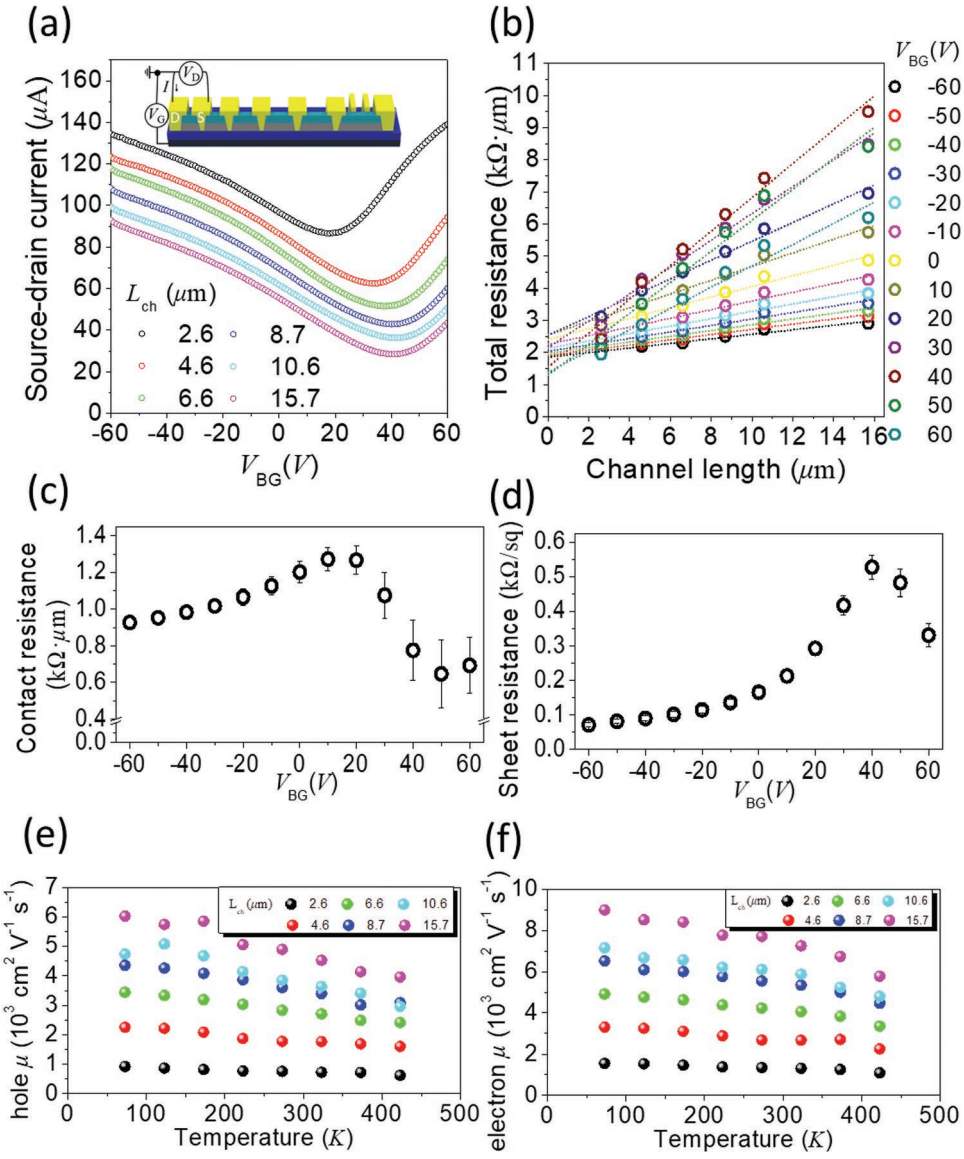

Figure 3. Electrical characteristics of edge-contacted graphene device of TLM structure. a) Transfer curves of edge-contacted graphene device at V_D = 0.1 V. b) TLM plot of the device with 2.7 μm channel width, measured at the gate voltage in the range of −60 to 60 V. c,d) R_c and R_{sh} of the device respectively. e,f) hole and electron mobilities of the device.

to TLM and 4PPM. To minimize the differences in electrical results under different experimental processing conditions, the devices were constructed on the same flake. **Figure 4**a,b shows R_{ch} and R_c of the surface- and edge-contacted few-layer graphene devices with Pd electrodes, measured by 4PPM. The results show high R_{ch} in the surface-contacted devices, while R_c is high in edge-contacted devices. This indicates the advantage in channel property resulted by using the edge-contacted devices, although R_c is high. In addition, note that Pd in contact with graphene causes a lower R_c than other metals because of its strong bonding and high work function.[7,12,36]

Here, it should be noted that ρ_c was calculated to be low for the edge-contacted graphene devices as shown in Figure 4c–f. This was due to carrier transport occurring at the effective contact area which gave rise to a large difference between edge and surface contacts as shown in Figure 4c,d. It is understood that carriers pass through over a part of the interfacial contact area when devices are in operation. The effective contact area for surface contact could be much larger than that for edge contact, due to the ultra-thinness of the 2D graphene channel. When comparing these two contact methods, the surface contact might show advantages with a larger contact area. However, newly calculated ρ_c with respect to the actual contact area is differently analyzed. The length by which the carriers mainly move across this reduced area is referred to L_T^*. By multiplying L_T^* by L_W, we can calculate the effective area, $A_{\text{surface contact}}$ (A_{SC}) = $W \times L_T^*$ as shown in Figure 4c. In contrast, L_T cannot be defined in edge contact, but it could be replaced with the thickness determined by the number of graphene layers because current flows across the thickness. More precisely, Figure 4d

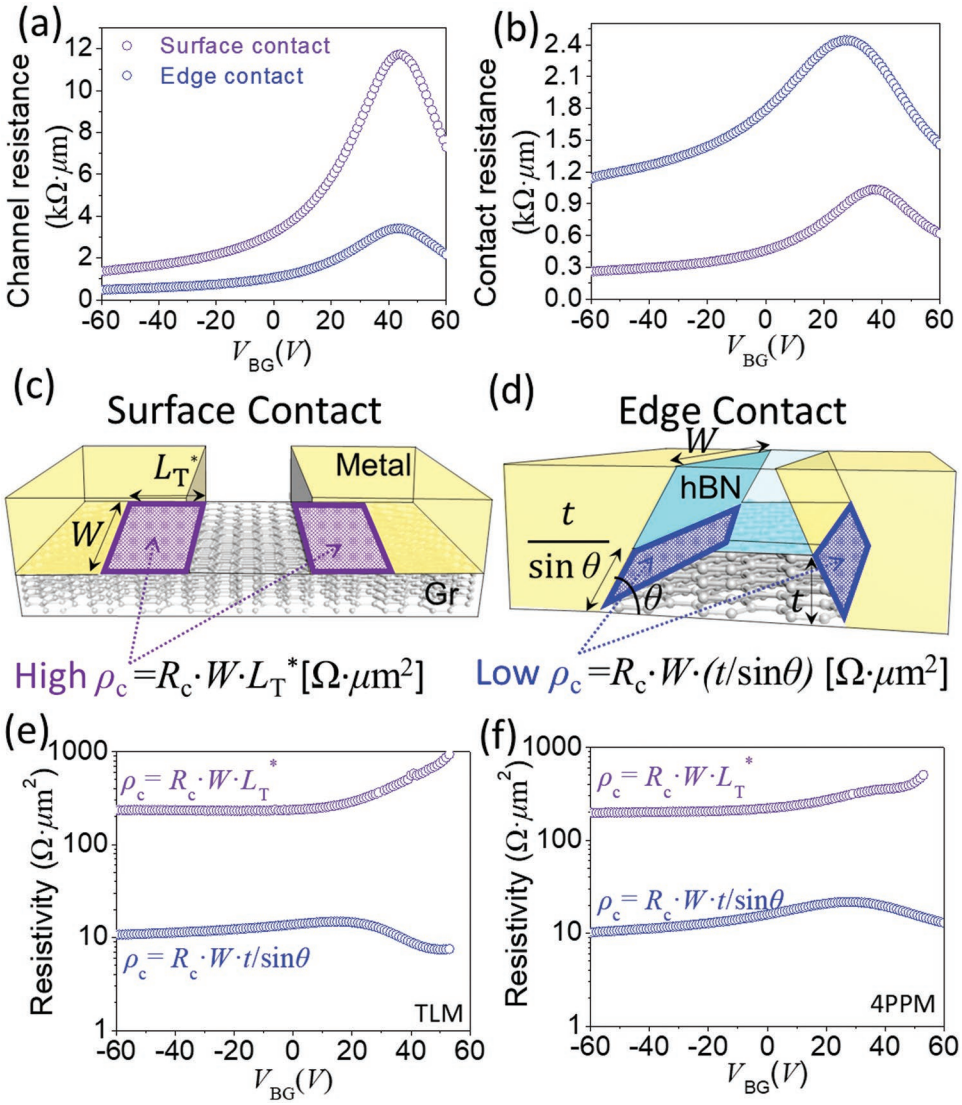

Figure 4. Comparison of electrical resistances and contact resistivities of graphene surface- and edge-contacted devices obtained by performing TLM and 4PPM. a) Comparison of R_{ch} of graphene surface- and edge-contacted devices obtained by 4PPM. b) Comparison of R_c of the devices obtained by 4PPM. c,d) Schematics showing effective current flowing cross-sectional areas for surface- and edge-contacted devices. e,f) ρ_c of surface- and edge-contacted devices obtained by performing TLM and 4PPM respectively.

shows the actual interfacing length should be determined by the thickness of few-graphene multiplied by etching slope (θ); that is, $1/\sin\theta$. In this case, the area where the actual charges are transported is estimated by $A_{\text{edge contact}}$ (A_{EC}) = $W \times t/\sin\theta$, where W is the thickness of the graphene channel. Thus, ρ_c is calculated by multiplying effective interfacing area to R_c, and ρ_c for edge or surface contact is then re-calculated with respect to interfacing area. In conclusion, we calculate the effective area which induces a 2D current flow for surface contact and the corresponding ρ_c using L_T^* obtained from the CER method as shown in Figure 4e (purple dots). We also calculate the effective area using graphene thickness instead of L_T^* for edge contact, as shown in Figure 4e (blue dots). Similarly, Figure 4f shows ρ_c obtained by 4PPM, for the two different contacts. Note that, in the case of 4PPM, we adopted L_T^* obtained from the TLM using the surface contact. Regardless of TLM or 4PPM, ρ_c for graphene FETs resulted in lower ρ_c in edge contact than surface contact.

2.4. Carrier Transport Analyzed by 3D Orbital and Band Diagram of Graphene

It is important to analyze data fairly because interfacing areas where effective charges are transported are very different depending on the contact method. It is understood that the carrier transport in few-layer graphene devices with an edge contact is rarely affected by the tunneling resistance between graphene and metal[18,39] due to the covalent bonding formed between metal and graphene. When the O_2 plasma reacts with graphene, oxygen molecules form bonds to carbon atoms in graphene. As the result, covalent bonding is achieved at the

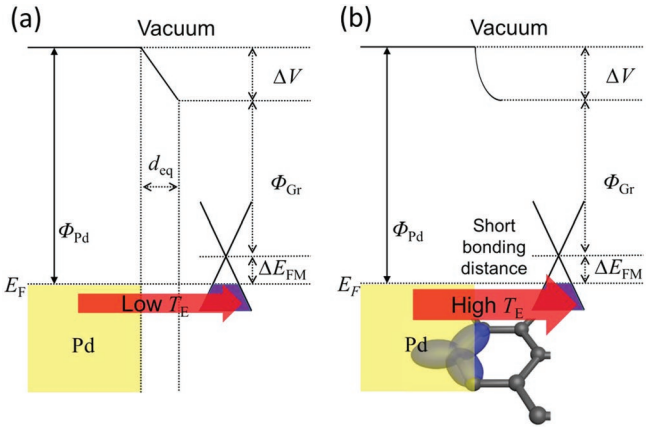

Figure 5. Schematics on band diagram and corresponding carrier transport at the metal interface of the graphene devices with different contacts, related to R_c and ρ_c. a) Surface contact and b) edge contact.

metal-graphene interface. That is, O_2 plasma treatment has improved R_c of the device because a defective part that covalently bonds metal to graphene is created.[34] Broken sp^2-hybridized C—C bonds are formed by O_2 plasma, but the broken bonds do not result in an increase in R_c but a decrease. These defects rather improve R_c to edge-contacted graphene devices.[25] **Figure 5**a,b are band diagrams with descriptive carrier transports that occur when two different contacts are made to the graphene channel, where E_{FM}, ΔV, and d_{eq} are the energy between the Dirac point and the Fermi level in metal-doped graphene, the total built-in potential, and the equilibrium distance, respectively. As shown in these figures, graphene has a hexagonal honeycomb structure in which the electron orbital shows a 3D structure with σ-bonds formed horizontally and π-bonds formed vertically. In the case of surface contact, $p\pi$ orbitals of carbon atoms contribute only to the metal-surface cohesion. However, in the case of edge contact, $p\sigma$ orbitals contribute to the surface cohesion and transmission because the surface carbon takes $p\sigma$ electrons with unpaired in zigzags or entailed in a weakened in-plane π bond in armchairs.[13,14] In addition, covalent bonds formed between metal and carbon atoms in the edge contact structure cause lower ρ_c compared to the surface contact structure which is dominated by weak van der Waals (vdW) force. Therefore, transmission efficiencies of edge-contacted devices of graphene are higher than surface-contacted devices.[8,21,24–26]

3. Conclusion

We found that, edge-contacted graphene devices show 23 times lower ρ_c (≈10 Ω μm^2) compared to surface-contacted graphene devices (≈230 Ω μm^2), after the normalization of the R_c results obtained from TLM and 4PPM on the surface-contacted and edge-contacted devices fabricated on the identical substrate with few-layer graphene. In this process, ρ_c of the surface-contacted device was measured more accurately by using L_T^* obtained from CER method of modified TLM. Also, this study demonstrates that, regardless of thickness of 2D materials it is possible to etch few-layer hetero-structures by plasma etching and therefore hetero-structured graphene devices can be developed by employing the edge contact.

4. Experimental Section

2D graphene and hBN were mechanically exfoliated on silicon wafer on a 285 nm SiO_2/p^{++} Si substrate after cleaning the wafer for 10 min in acetone and isopropyl alcohol (IPA) sequentially. These 2D samples exfoliated on the substrate were annealed at 300 °C for 1 h in a forming gas of 4% hydrogen in argon to remove remaining residues and to realize uniform 2D surface. The hetero-structure consisted of hBN and graphene was fabricated using a polycarbonate (PC) transfer method in which the processing temperature varied from 343 to 373 K for picking up the hBN. It was then fixed at 473 K for dropping down the hBN onto partial graphene where one part was used for surface contact and the other part is covered by hBN for edge contact. Residues formed by PC were then removed by chloroform.

The hetero-structure was coated using a resist which is formed by applying PMMA (A6 950 manufactured by Microchem) twice in a row at a speed of 4000 rpm for 60 s. It was then hardened at 180°C for 90 s. Patterns for 4PPM were defined using EBL (JEOL JSM-7001F and Raith ELPHY Plus & Quantum), after developing in a solution made up of IPA and deionized water (3:1). After rinsing with IPA and drying with nitrogen (N_2) gas, samples were etched by plasma using CF_4 (4 sccm) and O_2 (100 sccm) gases in the CCP mode at the following processing condition: working power, 80 W; pressure, 30 mTorr; and time, 60 s.

Electrodes were defined after forming contact metals by EBD (Korea Vacuum, KVE-E2000). Plasma etching was first performed for realizing edge contact with respect to the pattern drawn. Surface contact areas were subsequently formed by EBL. Thereafter, a 20 nm Pd/60 nm Au metal stack was deposited. Electrical measurements were carried out in a probe station after vacuum annealing at 473 K for 12 h (Agilent 4155C semiconductor analyzer and MSTECH vacuum probe station M6VC).

Supporting Information

Supporting Information is available from the Wiley Online Library or from the author.

Acknowledgements

S.L. and H.C. contributed equally to this work. This work was supported by the Global Research Laboratory (GRL) Program (2016K1A1A2912707), the Basic Science Research Program (2021R1A2C2010869), and the Global Frontier Research Program (2013M3A6B1078873), funded by National Research Foundation of Korea (NRF).

Conflict of Interest

The authors declare no conflict of interest.

Data Availability Statement

The data that support the findings of this study are available in the supplementary material of this article.

Keywords

2D graphene and hBN, contact resistance, contact-end-resistance, edge contact, four-point probe measurement, plasma etching, transmission line measurement

Received: December 7, 2021
Published online:

[1] G. Giovannetti, P. A. Khomyakov, G. Brocks, V. M. Karpan, J. Van Den Brink, P. J. Kelly, *Phys. Rev. Lett.* **2008**, *101*, 4.
[2] F. Léonard, A. A. Talin, *Nat. Nanotechnol.* **2011**, *6*, 773.
[3] D. Berdebes, T. Low, Y. Sui, J. Appenzeller, M. S. Lundstrom, *IEEE Trans. Electron Devices* **2011**, *58*, 3925.
[4] J. S. Moon, M. Antcliffe, H. C. Seo, D. Curtis, S. Lin, A. Schmitz, I. Milosavljevic, A. A. Kiselev, R. S. Ross, D. K. Gaskill, P. M. Campbell, R. C. Fitch, K. M. Lee, P. Asbeck, *Appl. Phys. Lett.* **2012**, *100*, 203512.
[5] C. Gong, G. Lee, B. Shan, E. M. Vogel, R. M. Wallace, K. Cho, *J. Appl. Phys.* **2010**, 108, 123711.
[6] C. Gong, D. Hinojos, W. Wang, N. Nijem, B. Shan, R. M. Wallace, K. Cho, Y. J. Chabal, *ACS Nano* **2012**, *6*, 5381.
[7] S. M. Song, J. K. Park, O. J. Sul, B. J. Cho, *Nano Lett.* **2012**, *12*, 3887.
[8] M. C. Lemme, L. J. Li, T. Palacios, F. Schwierz, *MRS Bull.* **2014**, *39*, 711.
[9] S. A. Peng, Z. Jin, P. Ma, D. Y. Zhang, J. Y. Shi, J. Bin Niu, X. Y. Wang, S. Q. Wang, M. Li, X. Y. Liu, T. C. Ye, Y. H. Zhang, Z. Y. Chen, G. H. Yu, *Carbon N. Y.* **2015**, *82*, 500.
[10] S. Venica, F. Driussi, A. Gahoi, P. Palestri, M. C. Lemme, L. Selmi, *IEEE Trans. Electron Devices* **2018**, *65*, 1589.
[11] T. Cusati, G. Fiori, A. Gahoi, V. Passi, M. C. Lemme, A. Fortunelli, G. Iannaccone, *Sci. Rep.* **2017**, *7*, 5109.
[12] J. Knoch, Z. Chen, J. Appenzeller, *IEEE Trans. Nanotechnol.* **2012**, *11*, 513.
[13] Y. Matsuda, W. Q. Deng, W. A. Goddard, *J. Phys. Chem. C* **2010**, *114*, 17845.
[14] Y. Khatami, H. Li, C. Xu, K. Banerjee, *IEEE Trans. Electron Devices* **2012**, *59*, 2453.
[15] K. Ito, T. Ogata, T. Sakai, Y. Awano, *Appl. Phys. Express* **2015**, *8*, 025101.
[16] L. Adamska, Y. Lin, A. J. Ross, M. Batzill, I. I. Oleynik, *Phys. Rev. B – Condens. Matter Mater. Phys.* **2012**, *85*, 195443.
[17] A. D. Franklin, S. J. Han, A. A. Bol, V. Perebeinos, *IEEE Electron Device Lett.* **2012**, *33*, 17.
[18] T. Chu, Z. Chen, *ACS Nano* **2014**, *8*, 3584.
[19] H. Y. Park, W. S. Jung, D. H. Kang, J. Jeon, G. Yoo, Y. Park, J. Lee, Y. H. Jang, J. Lee, S. Park, H. Y. Yu, B. Shin, S. Lee, J. H. Park, *Adv. Mater.* **2016**, *28*, 864.
[20] C. Gong, S. Mcdonnell, X. Qin, A. Azcatl, H. Dong, Y. J. Chabal, K. Cho, R. M. Wallace, *ACS Nano* **2014**, *1*, 642.
[21] Q. Gao, J. Guo, *APL Mater.* **2014**, *2*, 056105.
[22] J. T. Smith, A. D. Franklin, D. B. Farmer, C. D. Dimitrakopoulos, *ACS Nano* **2013**, *7*, 3661.
[23] S. Min Song, T. Yong Kim, O. Jae Sul, W. Cheol Shin, B. Jin Cho, *Appl. Phys. Lett.* **2014**, *104*, 183506.
[24] L. Wang, I. Meric, P. Y. Huang, Q. Gao, Y. Gao, H. Tran, T. Taniguchi, K. Watanabe, L. M. Campos, D. A. Muller, J. Guo, P. Kim, J. Hone, K. L. Shepard, C. R. Dean, *Science* **2013**, *342*, 614.
[25] D. W. Yue, C. H. Ra, X. C. Liu, D. Y. Lee, W. J. Yoo, *Nanoscale* **2015**, *7*, 825.
[26] A. Allain, J. Kang, K. Banerjee, A. Kis, *Electrical Contacts to Two-Dimensional Semiconductors*, Vol. *14*, Nature Publishing Group, London **2015**, pp. 1195–1205.
[27] F. Giubileo, A. Di Bartolomeo, *Prog. Surf. Sci.* **2017**, *92*, 143.
[28] D. S. Schulman, A. J. Arnold, S. Das, *Chem. Soc. Rev.* **2018**, *47*, 3037.
[29] A. Felten, A. Eckmann, J. J. Pireaux, R. Krupke, C. Casiraghi, *Nanotechnology* 355705, **2013**, *24*.
[30] S. Guo, M. Ghazinejad, X. Qin, H. Sun, W. Wang, F. Zaera, M. Ozkan, C. S. Ozkan, *Small* **2012**, *8*, 1073.
[31] I. Childres, L. A. Jauregui, J. Tian, Y. P. Chen, *New J. Phys.* **2011**, *13*, 025008.
[32] M. C. Prado, D. Jariwala, T. J. Marks, M. C. Hersam, *Appl. Phys. Lett.* **2013**, *102*, 193111.
[33] M. S. Choi, S. H. Lee, W. J. Yoo, *J. Appl. Phys.* **2011**, *110*, 073305.
[34] J. A. Robinson, M. Labella, M. Zhu, M. Hollander, R. Kasarda, Z. Hughes, K. Trumbull, R. Cavalero, D. Snyder, *Appl. Phys. Lett.* **2011**, *98*, 96.
[35] S. B. Mitta, M. S. Choi, A. Nipane, F. Ali, C. Kim, J. T. Teherani, J. Hone, W. J. Yoo, *Electrical Characterization of 2D Materials-Based Field-Effect Transistors*, Vol. *8*, IOP Publishing Ltd, Bristol, UK **2021**.
[36] F. Xia, V. Perebeinos, Y. M. Lin, Y. Wu, P. Avouris, *Nat. Nanotechnol.* **2011**, *6*, 179.
[37] S. Wang, D. Mao, Z. Jin, S. Peng, D. Zhang, J. Shi, X. Wang, *Nanotechnology* **2015**, *26*, 405706.
[38] K. I. Ho, C. H. Huang, J. H. Liao, W. Zhang, L. J. Li, C. S. Lai, C. Y. Su, *Sci. Rep.* **2014**, *4*, 5893.
[39] Y. Sui, J. Appenzeller, *Nano Lett.* **2009**, *9*, 2973.
[40] A. Hsu, H. Wang, K. K. Kim, J. Kong, T. Palacios, *IEEE Electron Device Lett.* **2011**, *32*, 1008.

